Journal of Sound and Vibration (1997) **203**(4), 641–665

NOISE SOURCE IDENTIFICATION IN A PROPFAN MODEL BY MEANS OF ACOUSTICAL NEAR FIELD MEASUREMENTS

F. Holste† and W. Neise

Deutsche Forschungsanstalt für Luft- und Raumfahrt e.V., Abteilung Turbulenzforschung, Berlin, Müller-Breslau-Str. 8, D-10623 Berlin, Germany

(*Received* 27 *November* 1995, *and in final form* 13 *December* 1996)

For the exploration of the dominant aerodynamic noise sources, the pressure fluctuations in the exit plane (near field) of the propfan model CRISP (Counter Rotating Integrated Shrouded Propfan) were measured with conventional 1/4 inch microphones. The pressure field of the tone components was resolved into a distribution of duct modes. Knowledge of the dominant modes allows conclusions about the dominant noise generation mechanisms, because the different noise sources inside the propfan create different sets of modes. The CRISP concept is developed by Motoren- und Turbinen-Union München (MTU). The experimental propfan has two counter-rotating rotors of 0·4 m diameter and equal speed. The shroud is supported by seven struts located downstream of the second rotor. Measurements were made with equal ($B_1 = B_2 = 10$) as well as unequal ($B_1/B_2 = 10/12$) blade numbers and under different operational conditions. The highest overall harmonic levels were found for the configuration with equal blade numbers. In this case, the blade passing frequency component is generated mainly by the rotor 2/struts interaction, and the higher blade tone harmonics, which dominate the overall tone noise level, are produced by the interaction of the two rotors. In the case of unequal blade numbers, all even harmonics of the shaft frequency ($H = 2, 4, 6, \ldots$) can be generated by the rotor 1/rotor 2 interaction. The harmonics below $H = 22$, however, are excited as non-propagational modes only and were found to have small amplitudes in the exit plane. The rotor 1/rotor 2 interaction is the main noise generation mechanism for the configuration with a short axial distance between the rotors. When the rotor distance is enlarged, the rotor/rotor interaction noise is reduced and, as a consequence, the contributions from the rotor/struts interactions become important. In addition to the experiments, a theoretical method is described for the prediction of the frequencies and azimuthal modes generated by two rotors with arbitrary speeds, directions of rotation and blade numbers. This method is helpful for the design of low noise rotor systems.

1. INTRODUCTION

In the next generation of civil aircraft engines, the bypass ratio will be increased to reduce the specific fuel consumption as well as the exhaust emissions. The bypass ratio of today's civil aircraft engines is of the order of 1:6. One conceptual design of future high bypass aircraft engines is schematically shown in Figure 1. The envisaged bypass ratio of the technology concept CRISP (Counter Rotating Integrated Shrouded Propfan), which is being developed by Motoren- und Turbinen Union München (MTU), is up to 1:20, with a predicted saving in specific fuel consumption of nearly 20%. The bypass flow is generated by two counter-rotating rotors, which are driven by a core engine. The shroud is supported

† Now at BMW Rolls-Royce AeroEngines, Eschenweg, D-15827 Dahlewitz, Germany.

0022–460X/97/240641 + 25 $25.00/0/sv960890

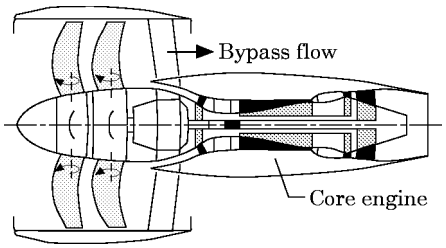

Figure 1. A schematic description of the CRISP aircraft engine.

by struts located downstream of the rotors. Guide vanes are not necessary in this design, because the swirl of the first rotor is removed by the second rotor. The core engine will be the same as in existing engines; only the rotor system driving the bypass flow is to be newly designed. A scaled down model with a 400 mm rotor diameter was constructed by MTU for aerodynamic and acoustic testing, and is shown in Figures 2 and 3. In the experimental model, the two counter-rotating rotors are driven by a compressed air turbine instead of a core engine.

The unsteady pressure field in the exit plane of the CRISP 0·4 m model is measured by using conventional 1/4 inch condenser microphones with nose cones. The spatial distribution of the complex pressures is then resolved into a distribution of acoustic duct modes with the following objectives.

(i) There are four source mechanisms which can be responsible for the blade passing frequency component and its harmonics. The first mechanism is the interaction between the inlet flow and the blade row of the first rotor; the second mechanism is the interaction between the two counter rotating rotors; the third is the interaction between the second rotor and the struts; and the fourth mechanism, finally, is the interaction between the wake flow from the first rotor, which is convected through the second blade row, and the struts. Each interaction process generates a characteristic set of spinning modes, and if the actual mode distribution in the exit plane is known, one can conclude what the dominant source mechanisms for the different tone components are.

(ii) Knowledge of the dominant spinning duct modes is also necessary to tune optimally the acoustic treatment (lining) of the shroud to achieve maximum noise reduction and, also, to devise efficient active noise control systems.

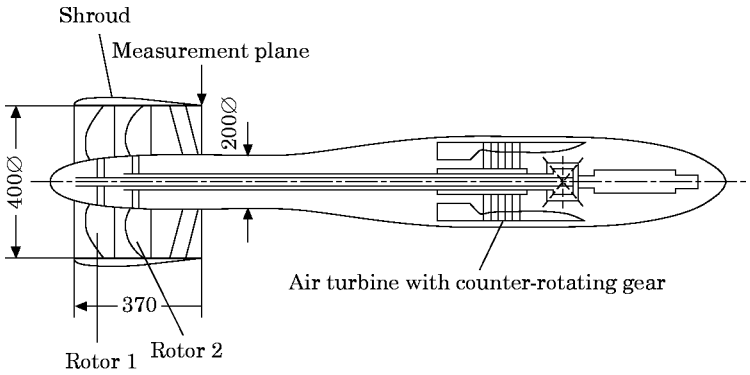

Figure 2. A schematic of the CRISP 0·4 m propfan model.

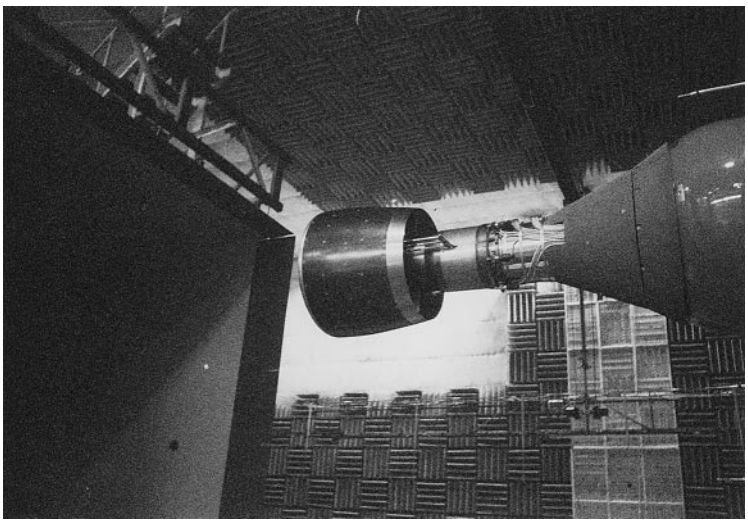

Figure 3. The experimental set-up in the open test section of the German–Dutch Wind Tunnel (DNW).

(iii) One can establish an experimental technique for assessing the tonal noise characteristics of aircraft engines which does not require ideal acoustic environmental conditions, i.e., free field conditions.

(iv) One can predict the sound pressure radiated into the far field based on the acoustic pressure modes measured in the acoustic near field; see the papers by Holste [1, 2]. The more detailed the experimental near field data are, the better is the accuracy of the predicted far field sound pressure.

The measurements were performed in the open test section of the German–Dutch Wind Tunnel (DNW, Deutsch Niederländischer Windkanal). In the first series of measurements, the CRISP model with two counter-rotating rotors of equal speed and blade numbers ($B_1 = B_2 = 10$) was studied; the axial distance between the rotors was $RD = 97{\cdot}3$ mm. To achieve a reduction in the tonal noise, unequal blade numbers were used on the two rotors for the second set of experiments, $B_1/B_2 = 10/12$; furthermore, two configurations with axial rotor distances of $RD = 97{\cdot}3$ mm and $RD = 177{\cdot}3$ mm were investigated. These propfan configurations were also tested in the DNW at different thrust conditions and wind tunnel speeds.

In section 2, the experimental mode analysis technique is presented together with a numerical simulation that shows the influence of measurement errors on the resultant mode distribution. A theoretical analysis is presented in section 3 for the frequency components and azimuthal duct modes generated by the interaction of two rotors of arbitrary speed (in both magnitude and direction) and blade numbers. This interaction model is helpful for the design of low noise rotor systems. Experimental results are presented in section 4 for the influence of the blade numbers and the axial distance between the two rotors on the frequency spectra and acoustic mode distributions generated in the exit plane.

2. TEST FACILITIES AND MODE ANALYSIS

The principal design of the propfan model is shown in Figure 2. The two rotors are $2R = 0{\cdot}4$ m in diameter and driven by a compressed air turbine via a spider gear. The shroud is supported by seven struts located downstream of the second rotor. The inner

diameter in the outlet plane is 0·4 m and the hub-to-tip ratio is 0·5. For the unsteady pressure measurements, a microphone traversing system was mounted directly on the hub behind the exit plane: see Figure 4. There are two microphone rakes placed on a rotatable cylinder at 180° angular distance. Six small DC motors and a gear drive were used to move the cylinder together with the microphones in the circumferential direction. With this arrangement, the pressure fluctuation were measured at 120 equally spaced angular positions ($\Delta\varphi = 3^\circ$). Each rake carries three 1/4 inch microphones with nose cones at the radial positions $r/R = 0{\cdot}96$, 0·785 and 0·61. The maximum flow Mach number in the exit plane is about $M = 0{\cdot}6$; the maximum wind tunnel flow Mach number is $M = 0{\cdot}22$.

2.1. DATA ACQUISITION AND MODE ANALYSIS

For the acoustic mode analysis, the circumferential and radial distributions of both the magnitude and phase of each spectral component of interest need to be known. Three two-channel FFT analyzers (HP-3562A) were used to measure the spectra of the six microphone signals. The analyzers were triggered by a one-pulse-per-revolution signal to obtain the averaged complex pressure spectra. In this way all non-rotational signal components, such as the turbulent pressure fluctuation of the jet flow, were suppressed. To eliminate leakage effects due to variations of the impeller speed, the sampling frequencies of the FFT analyzers were synchronized with the rotor speed. The complex frequency spectra were stored digitally for the numerical mode analysis, which could be carried out directly after completion of a circumferential traverse. For further analyses, all signals were stored on a digital tape recorder.

The numerical mode analysis used is described in references [2, 3] and can be summarized as follows. The sound pressure in the outlet plane can be resolved into azimuthal modes $A_m(r_j, \omega)$ for each frequency ω and each radial position r_j by using the relation

$$p_{s,j}(\omega) = \sum_{m=-\infty}^{\infty} A_m(r_j, \omega)\, \mathrm{e}^{\mathrm{i}m\varphi_s}. \tag{1}$$

Here the complex quantity $p_{s,j}(\omega)$ describes the measured pressure amplitude and phase at the radial position r_j and the circumferential positions φ_s.

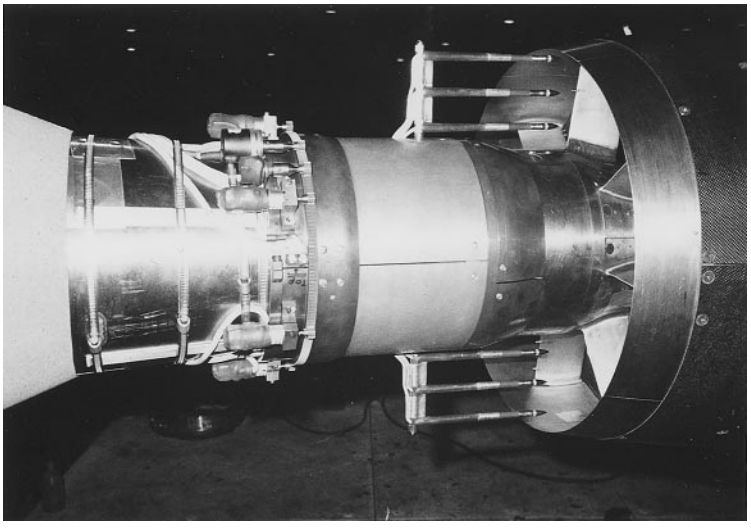

Figure 4. A view of the microphone traversing system mounted on the hub.

The Nyquist Sampling Theorem limits the range of azimuthal modes which can be determined from a set of experimental data. A mode can be determined uniquely if its azimuthal wavelength $2\pi/m$ is larger than twice of the distance $\Delta\varphi$ between adjacent measurement points. From this it follows, for the highest azimuthal mode order $m_g = |m_g|$,

$$2\pi/m_g > 2\Delta\varphi = 2(2\pi/N_\varphi) \Rightarrow m_g < N_\varphi/2. \tag{2}$$

N_φ is the number of measurement circumferential positions. In the present case, $N_\varphi = 120$ ($\Delta\varphi = 3^\circ$), and hence analysis of the azimuthal modes is possible in the range $m = -59$ to $m = 59$. If azimuthal modes of even higher order exist in the outlet plane, i.e., mode orders $|m_x| > N_\varphi/2$, an aliasing effect occurs, and these modes appear in the mode analysis range at the mode order $m = m_x + vN_\varphi$ with $v = \cdots -1, 0, 1. \ldots$

A discrete Fourier transform with respect to the circumferential angle φ was used to determine the azimuthal modes from the circumferential distribution of the complex pressure, for each radial position. Alternatively, a linear system of equations can be established and solved by using the least squares fit method.

In a second step the azimuthal modes with complex amplitudes $A_m(r_j, \omega)$ are expanded into a series of radial modes with complex amplitudes $A'_{mn}(\omega)$:

$$A_m(r_j, \omega) = \sum_{n=0}^{\infty} f_{mn}(\sigma_{mn} r_j/R) A'_{mn}(\omega),$$

$$f_{mn}(\sigma_{mn} r_j/R) = \mathrm{J}_m(\sigma_{mn} r_j/R) + Q_{mn}\,\mathrm{Y}_m(\sigma_{mn} r_j/R), \tag{3}$$

Here, J_m and Y_m are the Bessel and Neumann functions of order m, and the eigenvalues σ_{mn} and Q_{mn} can be determined by using the boundary condition of vanishing particle displacement at the rigid walls of hub and shroud. A linear system of equations was established for each azimuthal mode order m and solved by using the least squares fit method. Knowledge of the radial mode distribution $A'_{mn}(\omega)$ is necessary for prediction of the noise radiated into the acoustic far field (see references [1, 2]) as well as for the optimum design of active or passive noise control measures.

For the presentation of experimental results in section 4, the mode amplitudes A'_{mn} are normalized by

$$A^2_{mn} = (C_{mn}/R^2)|A'_{mn}|^2, \tag{4}$$

where

$$C_{mn} = \pi R^2[(1 - m^2/\sigma^2_{mn}) f^2_{mn}(\sigma_{mn}) - (\mu^2 - m^2/\sigma^2_{mn}) f^2_{mn}(\sigma_{mn}\mu)]. \tag{5}$$

μ is the ratio of the inner to the outer radius. The modal factor C_{mn} results from integrating the sound intensity over the exit plane of the propfan (see references [2, 4, 5]). The normalized mode amplitudes A_{mn} are representative of the modal sound power.

2.2. SIMULATION OF MEASUREMENT ERRORS

In the following, a theoretical simulation of measurement errors in both amplitude and phase is performed to check the accuracy of the mode analysis technique. First, the influence on azimuthal mode distributions is considered. Beginning with a given azimuthal mode distribution, which is depicted in Figure 5(a), the corresponding circumferential pressure distribution is calculated. Then random errors within $\pm 0{\cdot}5$ dB in amplitude and $\pm 5^\circ$ in phase are applied to the pressures at the respective measurement points, and an azimuthal mode analysis is performed with this set of simulated experimental data; the result is shown in Figure 5(b). The mode distribution shown in Figure 5(c) was obtained

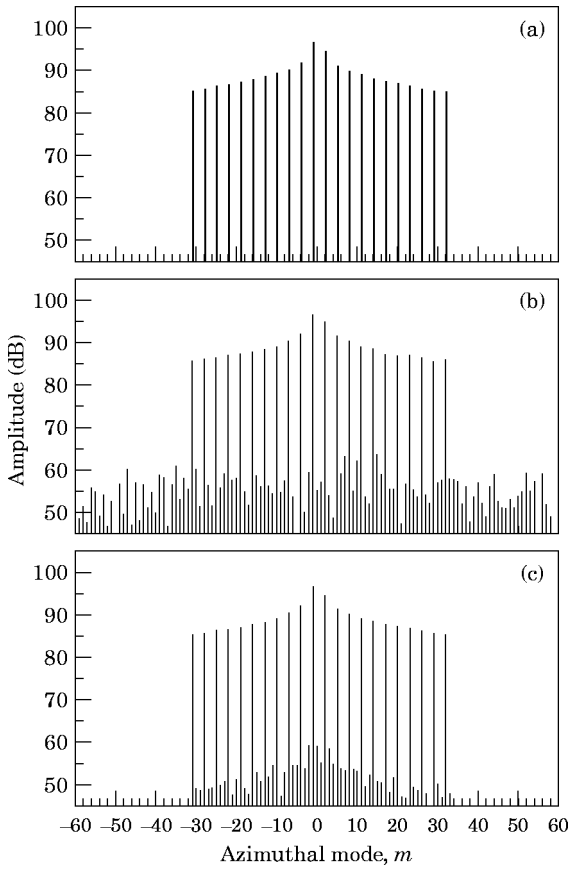

Figure 5. Simulation of measurement errors on the azimuthal mode distribution obtained from the numerical mode analysis technique. (a) No error simulation; (b) amplitude $\pm$ 0·5 dB and phase $\pm$ 5° uniformly distributed over all measurement points; (c) amplitude + 0·5 dB and phase + 5° added in the range of $\varphi^\circ = 183^\circ$–$360^\circ$.

by considering a constant measurement error of $\pm 0{\cdot}5$ dB in amplitude and $+5^\circ$ in phase for only the measurement points from $\varphi = 183^\circ$ to 360°; this was to simulate a mismatch between two microphones placed at the same radius but 180° apart; compare with the microphone traverse system described at the beginning of this section. The error simulation clearly shows that the original mode distribution is recovered by the present mode analysis technique, and that the amplitude and phase errors merely result in additional modes which have amplitudes of more than 30 dB below the original mode amplitudes.

A similar error simulation was also carried out for the radial mode analysis. The radial mode distribution depicted in Figure 6(a) was assumed to calculate the complex pressure amplitudes at the 360 circumferential measurement points ($\Delta\varphi = 3^\circ$) for the three radial distances $r/R = 0{\cdot}96$, $0{\cdot}785$ and $0{\cdot}61$ from the axis. A random error in the range of $\pm 0{\cdot}5$ dB in amplitude and $\pm 5^\circ$ in phase was applied to these pressures, and the radial mode analysis described in the foregoing was performed. The result is shown in Figure 6(b). Furthermore, to simulate errors in microphone calibration, a constant error of $\pm 0{\cdot}5$ dB in amplitude and 5° in phase was considered for all measurement points in the range from $\varphi = 183^\circ$ to 360°; the result of this exercise is shown in Figure 6(c). Similarly to the error simulation applied to the azimuthal mode analysis, the given modes appear almost unchanged in the mode distributions of Figures 6(b) and 6(c), and the additional

modes caused by the measurement errors have amplitudes more than 20 dB lower in level than the original ones.

The actual measurement errors are even smaller than in the above theoretical simulation, i.e., $\pm 0{\cdot}1$ dB in amplitude and $\pm 2^\circ$ in phase, so that the accuracy is better than shown in Figures 5 and 6.

3. AERODYNAMIC INTERACTION OF BLADE ROWS

The aerodynamic noise generation mechanism responsible for the tone noise generation of the CRISP propfan model have already been discussed in the introduction. The azimuthal modes produced by the interaction between the inlet flow and a rotor or between a rotor and guide vanes or struts are described in the Tyler and Sofrin famous paper [6], and the case of two counter-rotating rotors of equal speed and with equal blade numbers was treated by Holste and Neise [3]. Holste [2], finally, extended the analysis to the general case of rotor/rotor interaction with arbitrary blade numbers and rotor speeds, which includes the previous interaction models. Holste's model, which is described below, allows prediction of all tone frequencies and azimuthal mode orders which can be generated by the interaction of two arbitrary rotors. Therefore, it is highly useful for the design of low

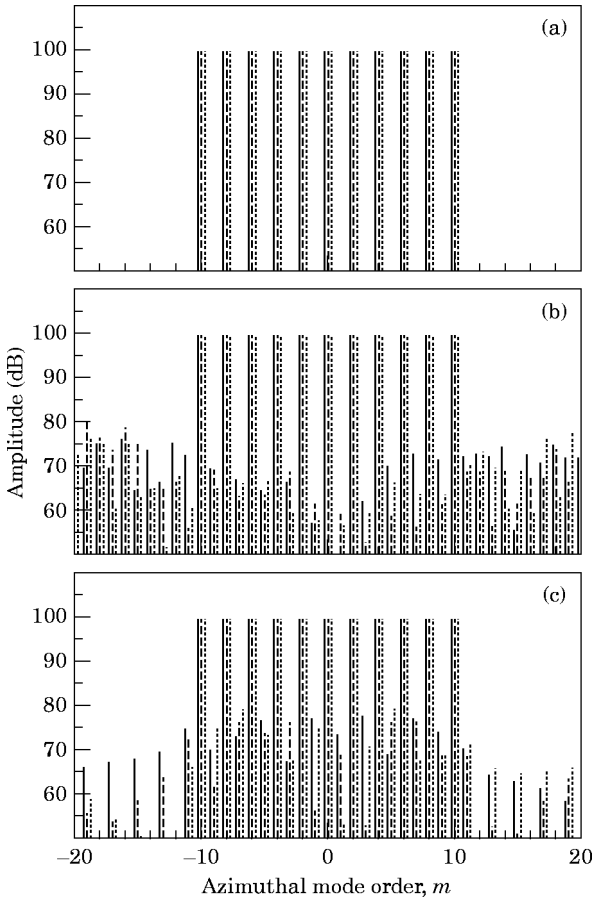

Figure 6. Simulation of measurement errors on the radial mode distribution obtained from the mode analysis technique. (a), (b), (c) as Figure 5. Radial mode order: ——, $n=0$; – – –, $n=1$; ---, $n=2$.

noise rotor systems, because the blade numbers and rotational speeds of the rotors can be selected in such a way that mainly non-propagational modes are excited, which have a poor radiation efficiency.

3.1. GENERAL CASE OF ROTOR/ROTOR INTERACTION

The two rotors considered have B_1 and B_2 blades, and their angular velocities are denoted by Ω_1 and Ω_2, respectively, where the mathematical sign indicates the direction of rotation. For a counter-rotating system, the signs of Ω_1 and Ω_2 are different.

The pressure field generated by the rotor/rotor interaction can be derived from the Tyler and Sofrin case of rotor/stator interaction by introducing a co-ordinate system φ_R which is attached to the second rotor. In this moving system of co-ordinates, the interactions between the rotors are the same as the interaction between a rotor and a stator, where the blades of the second rotor represent the stator vanes, and the speed of rotor 1 is equal to $\Omega_R = \Omega_1 - \Omega_2$. According to Tyler and Sofrin [6], the pressure field due to the interaction is given by

$$p^R(\varphi_R, t) = \sum_{h_R=-\infty}^{\infty} \sum_{m_R=-\infty}^{\infty} A_{m_R h_R}\, \mathrm{e}^{\mathrm{i}m_R\varphi_R}\, \mathrm{e}^{\mathrm{i}h_R B_1 \Omega_R t}$$

$$\text{with } m_R = k'B_2 - h_R B_1 \quad \text{and} \quad \Omega_R = \Omega_1 - \Omega_2. \tag{6}$$

Here, the quantities in the rotating system are denoted by the subscript R. $A_{m_R h_R}$ represents the amplitude of the azimuthal mode m_R generated at the blade tone harmonic h_R, which is observed in the co-ordinate system moving with the second rotor. $A_{m_R h_R}$ is zero for all $m_R \neq k'B_2 - h_R B_1$.

The circumferential angle φ as measured in the fixed frame of reference is related to the angle φ_R in the rotating system by

$$\varphi = \varphi_R + \Omega_2 t \Rightarrow \varphi_R = \varphi - \Omega_2 t. \tag{7}$$

Introducing this co-ordinate transformation into equation (6) yields the following expression for the pressure field in the fixed co-ordinate system,

$$p'(\varphi, t) = \sum_{h_R=-\infty}^{\infty} \sum_{m_R=-\infty}^{\infty} A_{m_R h_R}\, \mathrm{e}^{\mathrm{i}m_R\varphi}\, \mathrm{e}^{\mathrm{i}(h_R B_1 \Omega_R - m_R \Omega_2)t} \qquad \text{with } m_R = k'B_2 - h_R B_1, \tag{8}$$

and when the condition for m_R is inserted into the second exponent together with $\Omega_R = \Omega_1 - \Omega_2$ one obtains

$$p'(\varphi, t) = \sum_{h_R=-\infty}^{\infty} \sum_{m_R=-\infty}^{\infty} A_{m_R h_R}\, \mathrm{e}^{\mathrm{i}m_R\varphi}\, \mathrm{e}^{\mathrm{i}[h_R B_1 \Omega_1 - k'B_2\Omega_2]t} \qquad \text{with } m_R = k'B_2 - h_R B_1. \tag{9}$$

Here the mode order m_R and harmonic numbers h_R are defined in the rotating system. The usual expression for the pressure field of the tone components in the fixed co-ordinate system is

$$p'(\varphi, t) = \sum_{H=-\infty}^{\infty} \sum_{m=-\infty}^{\infty} A_{mH}\, \mathrm{e}^{\mathrm{i}m\varphi}\, \mathrm{e}^{\mathrm{i}H\Omega_g t}. \tag{10}$$

Ω_g is the fundamental frequency of the blade tone spectrum generated by the rotor/rotor interaction, which corresponds to the time period $T_g = 2\pi/\Omega_g$ after which the position of

the two rotors relative to one another is repeated. In case of counter-rotating systems with equal speed ($\Omega_1 = -\Omega_2$), the time period is equal to the time needed for one revolution, so that $T_g = 2\pi/\Omega_1$. If the rotational speeds are unequal, the relative positions of the rotor blades may repeat after more than one revolution. The numbers of revolutions necessary for each rotor to complete one period of the interaction pattern are denoted by u_1 and u_2. Since the time period T_g is equal to both rotors, one has the relation

$$u_1 T_1 = u_2 T_2 = T_g \qquad \text{with } T_1 = 2\pi/\Omega_1 \quad \text{and} \quad T_2 = 2\pi/\Omega_2. \tag{11}$$

Rearranging terms leads to

$$u_1(2\pi/\Omega_1) = u_2(2\pi/\Omega_2) = 2\pi/\Omega_g \Rightarrow \Omega_1 = u_1\Omega_g, \quad \Omega_2 = u_2\Omega_g, \tag{12}$$

where Ω_g is the largest common factor of the two rotor speeds Ω_1 and Ω_2, and u_1 and u_2 are integer values. Introducing equation (12) into equation (9) leads to

$$p'(\varphi, t) = \sum_{h_R=-\infty}^{\infty} \sum_{m_R=-\infty}^{\infty} A_{m_R h_R}\, \mathrm{e}^{\mathrm{i}m_R\varphi}\, \mathrm{e}^{\mathrm{i}(h_R B_1 u_1 - k' B_2 u_2)\Omega_g t} \qquad \text{with } m_R = k' B_2 - h_R B_1. \tag{13}$$

Comparison of equations (10) and (13) shows that $A_{m_R h_R} = A_{mH}$, and the conditions for H and m in the fixed co-ordinate system are

$$H = h_R B_1 u_1 - k' B_2 u_2 \qquad \text{and} \qquad m = k' B_2 - h_R B_1. \tag{14}$$

It is useful to introduce the highest common factor F_B (integer value) of the blade numbers B_1 and B_2:

$$b_1 = B_1/F_B, \quad b_2 = B_2/F_B \Rightarrow B_1 = F_B b_1, \quad B_2 = F_B b_2. \tag{15}$$

Inserting equations (15) into equation (14) and replacing h_R by $k'' = \ldots, -2, -1, 0, 1, 2, \ldots$, one obtains from equation (10), with $H = hF_B$ and $A_{mH} = A_{mh}$,

$$p'(\varphi, t) = \sum_{h=-\infty}^{\infty} \sum_{m=-\infty}^{\infty} A_{mh}\, \mathrm{e}^{\mathrm{i}m\varphi}\, \mathrm{e}^{\mathrm{i}hF_B\Omega_g t} \qquad \text{with the conditions } \begin{Bmatrix} m = F_B(k' b_2 - k'' b_1) \\ h = k'' b_1 u_1 - k' b_2 u_2 \end{Bmatrix}. \tag{16}$$

Equation (16) reveals that, for blade number combinations with $F_B > 1$, not all harmonics of Ω_g are generated by the rotor/rotor interaction, but only multiples of $F_B\Omega_g$. This means that the fundamental frequency is $F_B\Omega_g$ ($h = 1$) instead of Ω_g. In other words, the time period of the interaction process is reduced from T_g to $T' = T_g/F_B$, because the interference pattern of the two blade rows is repeated every T' instead of T_g. Also, the azimuthal order m of the generated modes is restricted in that m can be only multiples of F_B. This means that for designing low noise rotor systems a blade number combination with a high common factor F_B (see equation (15)) should be chosen, so that the number of propagational modes is minimized. The above conclusions are valid for counter-rotating as well as for co-rotating rotor systems.

By using equations (12) and (15), equation (16) can be rewritten as

$$p'(\varphi, t) = \sum_{H=-\infty}^{\infty} \sum_{m=-\infty}^{\infty} A_{mH}\, \mathrm{e}^{\mathrm{i}m\varphi}\, \mathrm{e}^{\mathrm{i}H\Omega_g t} \quad \text{with the conditions } \begin{Bmatrix} m = k' B_2 - k'' B_1 \\ H\Omega_g = k'' B_1 \Omega_1 - k' B_2 \Omega_2 \end{Bmatrix}. \tag{17}$$

Here the conditions for the generated modes m and frequencies $H\Omega_g$ depend directly on the blade numbers B_1/B_2 and on the rotor speeds Ω_1/Ω_2.

3.2. INTERACTION OF COUNTER-ROTATING ROTORS WITH EQUAL SPEEDS

In the following, the case of the CRISP propfan studied experimentally is considered. The condition $\Omega_1 = -\Omega_2$ leads to $\Omega_g = \Omega$, $u_1 = 1$ and $u_2 = -1$. Introducing these relations into equation (16) gives

$$p'(\varphi, t) = \sum_{h=-\infty}^{\infty} \sum_{m=-\infty}^{\infty} A_{mh}\, \mathrm{e}^{\mathrm{i}m\varphi}\, \mathrm{e}^{\mathrm{i}hF_B\Omega t} \qquad \text{with the conditions } \begin{Bmatrix} m = F_B(k'b_2 - k''b_1) \\ h = k''b_1 + k'b_2 \end{Bmatrix}. \quad (18)$$

3.2.1. *Equal blade numbers*

For $B_1 = B_2 = B$, $F_B = B$, with $b_1 = b_2 = 1$, and the conditions in equation (18) become

$$m = B(k' - k'') \qquad \text{and} \qquad h = k' + k''. \quad (19)$$

The expression $k' + k''$ yields all integer numbers for h by arbitrary values of k' or k''. h is the harmonic order of the fundamental frequency $B\Omega$. To obtain m as a function of h, the two expressions in equation (19) are combined:

$$m = B(2k' - h). \quad (20)$$

As is to be expected, only the blade passing frequency $B\Omega$ and its harmonics can be generated in this case. In the mode distribution of all harmonics, the azimuthal mode orders m generated are spaced by two times the blade number B.

3.2.2. *Unequal blade numbers*

Combining the expression for m and h in equation (18) leads to

$$m = F_B(2k'b_2 - h) \qquad \text{with } h = k'b_2 + k''b_1. \quad (21)$$

In this relationship, k' and k'' cannot assume arbitrary integer values for a given harmonic h, if $b_1 > 1$ and $b_2 > 1$. Therefore, the distance Δm in the mode distribution generated between two adjacent modes must be larger than $2k'F_Bb_2$. For $h = 0$ the generated mode orders can be easily derived from equation (21):

$$0 = k'b_2 + b_1k'' \Rightarrow k'b_2 = -b_1k'' \Rightarrow k' = wb_1, \quad k'' = -wb_2 \quad \text{with } w = \ldots, -1, 0, 1, \ldots. \quad (22)$$

Introducing this expression for k' into equation (21) gives, with $h = 0$,

$$m = 2wF_Bb_1b_2. \quad (23)$$

This equation shows that the distance between modes is $\Delta m = 2F_Bb_1b_2$. $h = 0$ represents the case of zero frequency: i.e., the steady component of the pressure field which does not contribute to the sound radiation. However, it is expected here that a similar series of modes is generated for all other harmonics h as well. Therefore, k' and k'' in equation (21) are expressed as

$$k' = wb_1 + s'_h, \qquad k'' = -wb_2 - s''_h. \quad (24)$$

Introducing equations (24) into equation (21) yields

$$h = s'_hb_2 - s''_hb_1, \qquad m = F_B(2wb_1b_2 + 2s'_hb_2 - h). \quad (25)$$

s'_h and s''_h can be interpreted as "starting values" for the series k' and k'' for each harmonic h, which means that no unique values exist. However, it is sufficient to know one pair of values (s'_h, s''_h) for each harmonic to describe the entire series. Additionally, equation (25)

shows that the distance between mode orders in the mode distribution generated is equal to $2F_B b_1 b_2$ for each harmonic.

Finally, the pressure field of two coupled counter-rotating rotors is given by ($\Omega = \Omega_1 = -\Omega_2$):

$$p'(\varphi, t) = \sum_{h=-\infty}^{\infty} \sum_{w=-\infty}^{\infty} A_{mh}\, \mathrm{e}^{\mathrm{i}m\varphi}\, \mathrm{e}^{\mathrm{i}hF_B\Omega t}$$

$$\text{with } h = s'_h b_2 - s''_h b_1 \quad \text{and} \quad m = F_B(2wb_1b_2 + 2s'_h b_2 - h), \tag{26}$$

where m cannot assume all integer numbers.

3.3. FREQUENCY COMPONENTS AND AZIMUTHAL MODES GENERATED BY THE CRISP PROPFAN WITH COUNTER-ROTATING ROTORS WITH EQUAL SPEEDS AND DIFFERENT BLADE NUMBERS

In Table 1 are listed the conditions for the frequency components and azimuthal modes m which can be generated by the different interaction processes in the present CRISP 0·4 m propfan model: i.e., for the case of counter-rotation at equal speeds. Here, h denotes the harmonics of a fundamental frequency, V is the number of struts, k, k' and k'' are integers, and F_B is the largest common factor of the blade numbers B_1 and B_2. For the blade number combination $B_1/B_2 = 10/12$, $F_B = 2$, which means that all even harmonics of the shaft frequency can be generated by the rotor 1/rotor 2 interaction.

The frequencies and mode orders m, which can be generated by the various interaction processes relevant to the CRISP propfan model with $B_1/B_2 = 10/12$ blades, are listed in Table 2. H is the harmonic order of the shaft frequency. The frequencies of the harmonics H, which are listed in the last but one column, are for the maximum rotor speed of 12 000 r.p.m. In the last column, the magnitudes of the highest azimuthal order ($|m|$, 0) of the modes are given, which are propagational in the annulus of the propfan's exit plane at the frequency of the harmonic H considered. The cut-on frequency of a mode (m, n) increases with the radial mode order n ($n > 0$). In the list of modes generated by the various interaction mechanisms, the mode order numbers printed in bold italic characters correspond to propagational azimuthal modes (m, 0). At lower rotor speeds, the frequencies of the harmonics decrease, and the number of propagational modes is diminished in turn.

An expected result in Table 2 is that the interactions rotor 1/struts and rotor 2/struts generate shaft order harmonics equal to multiples of the blade numbers B_1 and B_2,

TABLE 1

Summary of conditions for the frequency components and azimuthal modes m generated by the propfan model with counter-rotating rotors of equal speed

Source mechanism	Frequency	Mode order m
Uniform inlet flow/rotor 1	$hB_1\Omega$	$m = hB_1$
Rotor 1/struts	$hB_1\Omega$	$m = hB_1 + kV$
Rotor 2/struts	$hB_2\Omega$	$m = -hB_2 + kV$
Rotor 1/rotor 2		
Equal blade number, $B_1 = B_2 = B$	$hB\Omega$	$m = B(2k - h)$
Unequal blade number, $B_1 = F_B b_1$, $B_2 = F_B b_2$	$hF_B\Omega$	$\left.\begin{matrix} m = F_B(k'b_2 - k''b_1) \\ h = k''b_1 + k'b_2 \end{matrix}\right\}$

respectively. The azimuthal mode orders of subsequent modes are spaced by $\Delta m = 7$, which is equal to the number of struts. The interaction between the two counter-rotating rotors generates all even harmonics of the shaft frequency, including multiples of B_1 and

TABLE 2

A list of the shaft order harmonics H and azimuthal mode orders m generated by the propfan model CRISP with unequal blade numbers

Blade numbers $B_1 = 10$, $B_2 = 12$; H, harmonic of the shaft frequency; shaft frequency = 200 Hz; $F_B = 2$, $b_1 = 5$, $b_2 = 5$

	Azimuthal modes m generated by the interactions															
H	Rotor 1/rotor 2				Rotor 2/struts					Rotor 1/struts					Frequency (kHz)	m cut-on
2	−218	−98	22	142	—	—	—	—	—	—	—	—	—	—	0·4	1
4	−196	−76	44	164	—	—	—	—	—	—	—	—	—	—	0·8	2
6	−174	−54	66	186	—	—	—	—	—	—	—	—	—	—	1·2	3
8	−152	−32	88	208	—	—	—	—	—	—	—	—	—	—	1·6	4
10	−130	−10	110	230	—	—	—	—	—	−17	−10	***−3***	***4***	11	2	5
12	−228	−108	12	132	−9	***−2***	***5***	12	19	—	—	—	—	—	2·4	7
14	−206	−86	34	154	—	—	—	—	—	—	—	—	—	—	2·8	8
16	−184	−64	56	176	—	—	—	—	—	—	—	—	—	—	3·2	9
18	−162	−42	78	198	—	—	—	—	—	—	—	—	—	—	3·6	11
20	−140	−20	100	220	—	—	—	—	—	−20	−13	***−6***	***1***	***8***	4	12
22	−118	***2***	122	242	—	—	—	—	—	—	—	—	—	—	4·4	14
24	−216	−96	24	144	***−11***	***−4***	***3***	***10***	17	—	—	—	—	—	4·8	15
26	−194	−74	46	166	—	—	—	—	—	—	—	—	—	—	5·2	16
28	−172	−52	68	188	—	—	—	—	—	—	—	—	—	—	5·6	18
30	−150	−30	90	210	—	—	—	—	—	***−16***	***−9***	***−2***	***5***	***12***	6	19
32	−128	***−8***	112	232	—	—	—	—	—	—	—	—	—	—	6·4	21
34	−106	***14***	134	254	—	—	—	—	—	—	—	—	—	—	6·8	22
36	−204	−84	36	156	***−13***	***−6***	***1***	***8***	***15***	—	—	—	—	—	7·2	24
38	−182	−62	58	178	—	—	—	—	—	—	—	—	—	—	7·6	25
40	−160	−40	80	200	—	—	—	—	—	***−19***	***−12***	***−5***	***2***	***9***	8	26
42	−138	***−18***	102	222	—	—	—	—	—	—	—	—	—	—	8·4	28
44	−116	***4***	124	244	—	—	—	—	—	—	—	—	—	—	8·8	29
46	−94	***26***	146	266	—	—	—	—	—	—	—	—	—	—	9·2	31
48	−192	−72	48	168	***−8***	***−1***	***6***	***13***	***20***	—	—	—	—	—	9·6	32
50	−170	−50	70	190	—	—	—	—	—	***−15***	***−8***	***−1***	***6***	***13***	10	34
52	−148	***−28***	92	212	—	—	—	—	—	—	—	—	—	—	10·4	35
54	−126	***−6***	114	234	—	—	—	—	—	—	—	—	—	—	10·8	36
56	−104	***16***	136	256	—	—	—	—	—	—	—	—	—	—	11·2	38
58	−82	***38***	158	278	—	—	—	—	—	—	—	—	—	—	11·6	39
60	−180	−60	60	180	***−10***	***−3***	***4***	***11***	***18***	***−18***	***−11***	***−4***	***3***	***10***	12	41
62	−158	***−38***	82	202	—	—	—	—	—	—	—	—	—	—	12·4	42
64	−136	***−16***	104	224	—	—	—	—	—	—	—	—	—	—	12·8	44
66	−144	***6***	126	246	—	—	—	—	—	—	—	—	—	—	13·2	45
68	−92	***28***	148	268	—	—	—	—	—	—	—	—	—	—	13·6	46
70	−70	50	170	290	—	—	—	—	—	***−14***	***−7***	***0***	***7***	***14***	14	48
72	−168	***−48***	72	192	***−12***	***−5***	***2***	***9***	***16***	—	—	—	—	—	14·4	49
74	−146	***−26***	94	214	—	—	—	—	—	—	—	—	—	—	14·8	50
76	−124	***−4***	116	236	—	—	—	—	—	—	—	—	—	—	15·2	52
78	−102	***18***	138	258	—	—	—	—	—	—	—	—	—	—	15·6	53
80	−80	***40***	160	280	—	—	—	—	—	***−17***	***−10***	***−3***	***4***	***11***	16	55

B_2. At each of these harmonics, the difference in the azimuthal order of subsequent modes Δm is 120.

Most of the shaft order harmonics listed in Table 2 are produced by only one of the three interaction mechanisms involved. Overlapping occurs at $H = 60$ (interactions rotor 1/struts and rotor 2/struts) and at the shaft orders equal to multiples of the two blade numbers. At the frequencies where overlapping is observed of the interactions rotor 1/struts, rotor 2/struts, and rotor 1/rotor 2, the latter produces only non-propagational modes, except for $H = 72$, the amplitudes of which decay while propagating from the rotors to the exit plane.

The result of this analysis applied to the present test configuration shows that the interaction between two counter-rotating rotors of equal speed and with $B_1 = 12$, $B_2 = 10$ blades produces all even harmonics of the rotor shaft frequency: i.e., $H = 2, 4, 6$. On the other hand, all rotor harmonics below the order $H = 22$ are generated as acoustic duct modes with high azimuthal mode order which cannot propagate in the annular engine duct and therefore can be expected to have small amplitudes in the exit plane.

4. EXPERIMENTAL RESULTS

4.1. GENERAL REMARKS

Initial tests with the CRISP 0·4 m model have shown that the microphone probes placed in the jet flow do not interfere with the blade tone harmonic noise. Also, it was found that the turbulence intensity of the wind tunnel flow has no measurable influence on the tone components radiated.

In section 4.2 "typical" mode distributions for the first six blade tone harmonics are shown for the case of equal blade numbers on both rotors, and in section 4.3 the results obtained with the blade numbers $B_1/B_2 = 10/12$ and with two axial distances between the rotors are discussed. A comparison of the overall tone noise levels of the three propfan configurations tested is given in section 4.4. Radial mode distributions are presented in section 4.5.

4.2. EQUAL BLADE NUMBERS

In Figure 7 is shown the conventional pressure spectrum, i.e., averaged in the frequency domain, measured at an arbitrary measurement point in the exit plane for the case of equal blade numbers ($B_1 = B_2 = 10$). The operational condition of the propfan was representative of take-off conditions, with a relative pressure ratio of $\pi_{rel} = 0{\cdot}8$. π_{rel} characterizes the engine thrust, with $\pi_{rel} = 1$ at full thrust. As expected, the blade passing frequency ($B \times \Omega$) and multiples thereof dominate the spectrum. At this measurement point, the second, third and fourth harmonics have the highest amplitudes, which mainly contribute to the overall noise level in the radiated far field. For more information about the far field noise; see the paper by Dobrzynski *et al*. [7].

The azimuthal mode distributions for various tone components generated in the exit plane were determined for different operation conditions of the propfan model. Typical azimuthal mode distributions are shown in Figure 8 for the first six blade tone harmonics. The blade stagger angle is the same for both rotors, $\beta = -6^\circ/-6^\circ$, the wind tunnel flow Mach number is $M = 0{\cdot}22$ at zero angle of attack, $\alpha = 0$, and the relative pressure ratio of the fan is $\pi_{rel} = 1$ (maximum thrust). The mode distributions measured on different radial distances from the axis are labelled by different line symbols, while the various point symbols indicate which interaction mechanism is responsible for the particular azimuthal

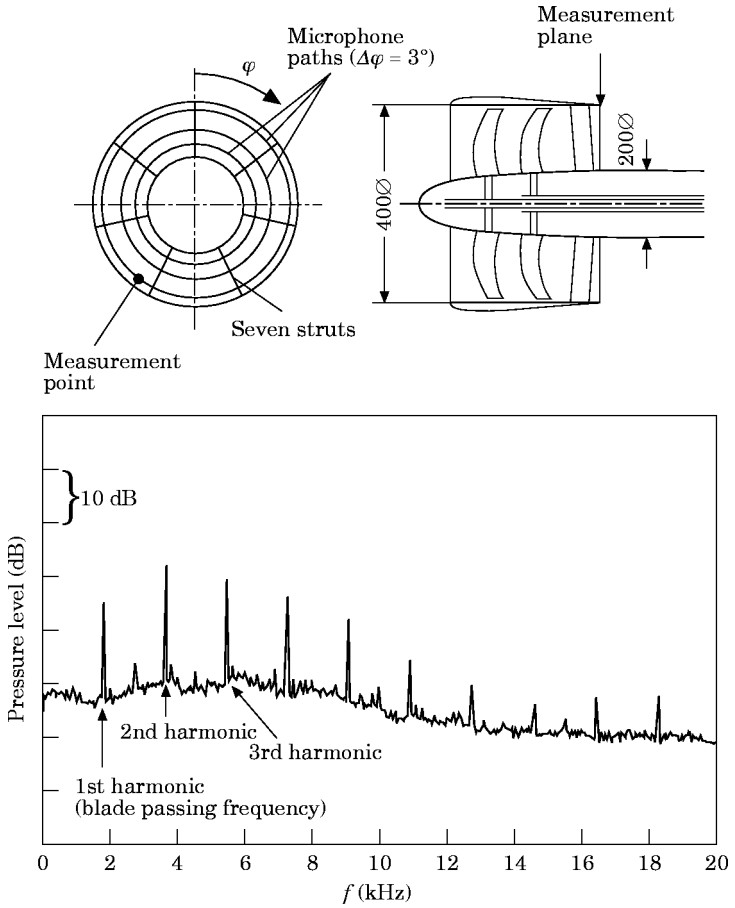

Figure 7. The sound pressure spectrum in the outlet plane of the CRISP 0·4 m model; $B_1 = B_2 = 10$, $RD = 97{\cdot}3$ mm.

mode. Two vertical arrows in each graph mark the range of propagational modes in the annulus between shroud and hub.

For all harmonics, only propagational modes occur in the exit plane, the other modes are of much lower amplitude. This indicates that the shroud helps reduce the noise in comparison with unducted propfans. For all blade tone harmonics, the mode distributions obtained for the three radial distances from the axis exhibit the same characteristic behaviour: i.e., the dominant modes are the same at all three radii. The amplitude of a particular azimuthal mode depends on the radial position, which indicates that higher radial modes exist, as will be shown in section 4.5.

At some blade tone harmonics, modes occur which are neither generated by the interaction between the two rotors nor by the interaction between a rotor and the struts. As was shown by Zandbergen *et al*. [8], these modes are formed by a transformation of modes at the struts. For example, a mode that is generated by the rotor 1/rotor 2 interaction is propagated downstream until it impinges on the struts. Due to its rotation, it interacts with the struts just like a rotor wake. As a result, this mode is spread into a series of modes, the order numbers of which are spaced by the strut number.

While most of the blade tone harmonics are generated by the interaction between the counter-rotating blade rows, this is not true for the blade passing frequency component.

At this frequency, the rotor 1/rotor 2 interaction produces only evanescent modes, the strongest of which are $m = -10$ and $m = 10$. The dominant modes at the blade passing frequency are $m = 3$ and $m = -4$; the most likely cause of these is the interaction between rotor 2 and struts; however, they can also be generated by the transformation of mode $m = 10$ at the struts. In any case, enlarging the distance between rotor 2 and the struts would lower the blade passing frequency level substantially, because it would weaken both possible source mechanisms involved: (1) the wakes from the second blade row would wash out more over a longer distance; and (2) the non-propagational mode $m = 10$ produced by the rotor/rotor interaction would decay more. In both cases the interaction forces on the struts would be diminished.

In the mode distributions of the second harmonic, the mode $m = 0$ generated by the interaction between the two rotors dominates the sound field and is mainly responsible for the noise radiation at this tone component. The second most important modes $m = -6$ and $m = 13$ are produced either by the rotor 2/struts interaction or, less likely, by the transformation of the mode $m = 20$ at the struts.

The mode distributions for the blade tone harmonics 3–6 show that modes which were produced by a mode transformation at the struts can have amplitudes almost as high or even higher than the primary mode. For example at the third blade tone harmonic, the modes $m = -17$, 11, 18 originate from the mode $m = -10$; and similarly, for the fourth harmonic, the modes $m = -27$, -13, 15, 22, 29 from $m = -20$, and $m = -22$, 13, 27 from $m = 20$.

It is obvious from the above discussion that the levels of the blade tone harmonics 2–6 can be reduced most efficiently by increasing the distance between the two rotors. Also, unequal numbers of blades should be used, so that interaction modes with high mode orders are generated, which have a lower acoustic radiation efficiency than the low order ones.

4.3. UNEQUAL BLADE NUMBERS

In Figure 9 is shown a pressure spectrum measured in the outlet plane of the propfan model with unequal blade numbers $B_1/B_2 = 10/12$. In agreement with the theoretical considerations presented in section 3.3, the dominant tone components are the even harmonics of the shaft frequency Ω. For these harmonics, the azimuthal mode distributions were calculated, and three examples are depicted in Figure 10; i.e., for the 10th, 24th and 32nd shaft orders. The shaft rotational frequency was 186·1 Hz and the axial distance between the rotors was $RD = 97{\cdot}3$ mm. The range of propagational modes is indicated by two vertical arrows. Clearly, the mode distributions in the exit plane are dominated by these propagational modes. Note that the mode orders of the propagational modes predicted in Table 2 are exactly the ones with the highest amplitudes in Figure 10. The mode $m = -8$, produced by the rotor 1/rotor 2 interaction, has the highest amplitude in the mode distribution for the shaft order $H = 32$. The presence of the modes $m = -22$, -15 and $m = 13$, 20 cannot be explained by any of the interaction mechanism discussed above, but only by a mode transformation due to the interaction of the mode $m = -8$ with the struts. Similar effects were already shown for the case of equal blade numbers in section 4.2 and in reference [3].

In Figure 10, modes due to the rotor 1/struts or rotor 2/struts interactions are present only in the mode distributions of the shaft orders $H = 10$ and $H = 24$. However, these modes may also be generated by a mode transformation at the struts. This effect can be illustrated by using the mode distribution of the shaft harmonic order $H = 10$. The mode $m = -10$ is generated by the rotor 1/struts interaction as well as by the rotor 1/rotor 2 interaction. The mode $m = -10$ does not propagate and therefore decays exponentially

with increasing distance from the rotor. Nevertheless, it may still be strong enough to interact with the struts, because the distance between the rotors and the struts is fairly short, and as a result propagational modes of the orders $m = -3$ and 4 are produced. Similar effects can be observed at other shaft order harmonics; compare the cases $H = 12$, 24, ... and $H = 20$, 30, ... in Table 2. The above discussion has shown that, for some tone components, a unique determination of the main source mechanisms is not possible,

(a)

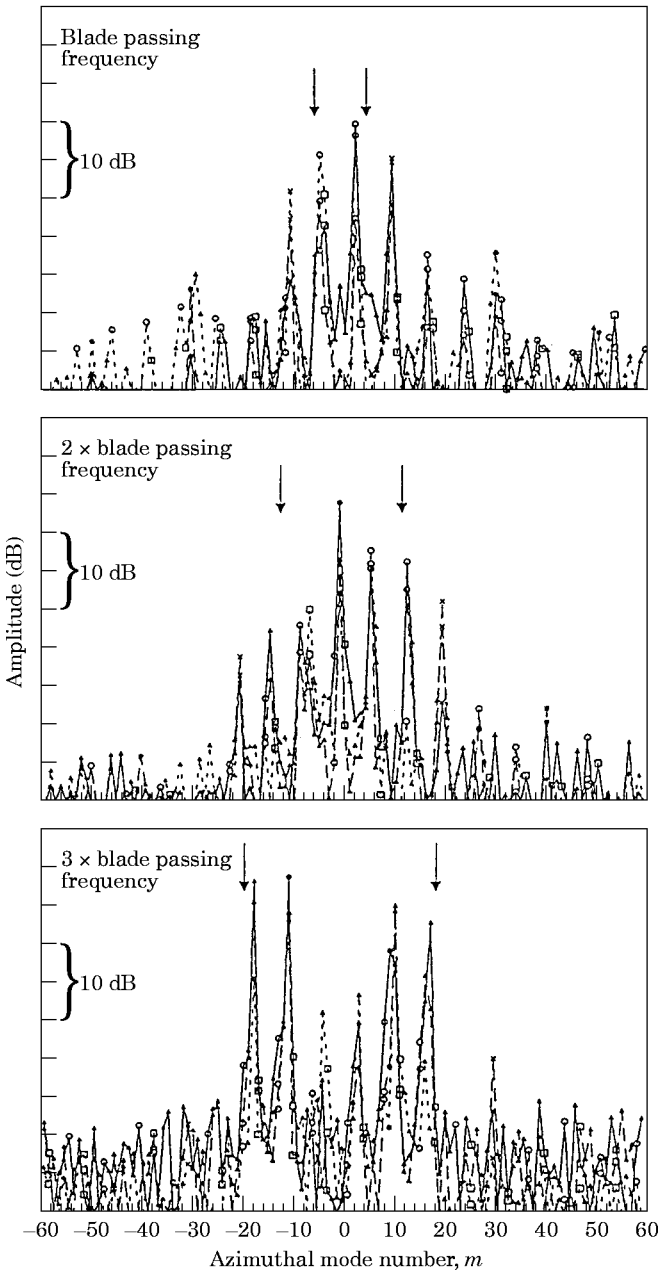

Fig. 8a

(b)

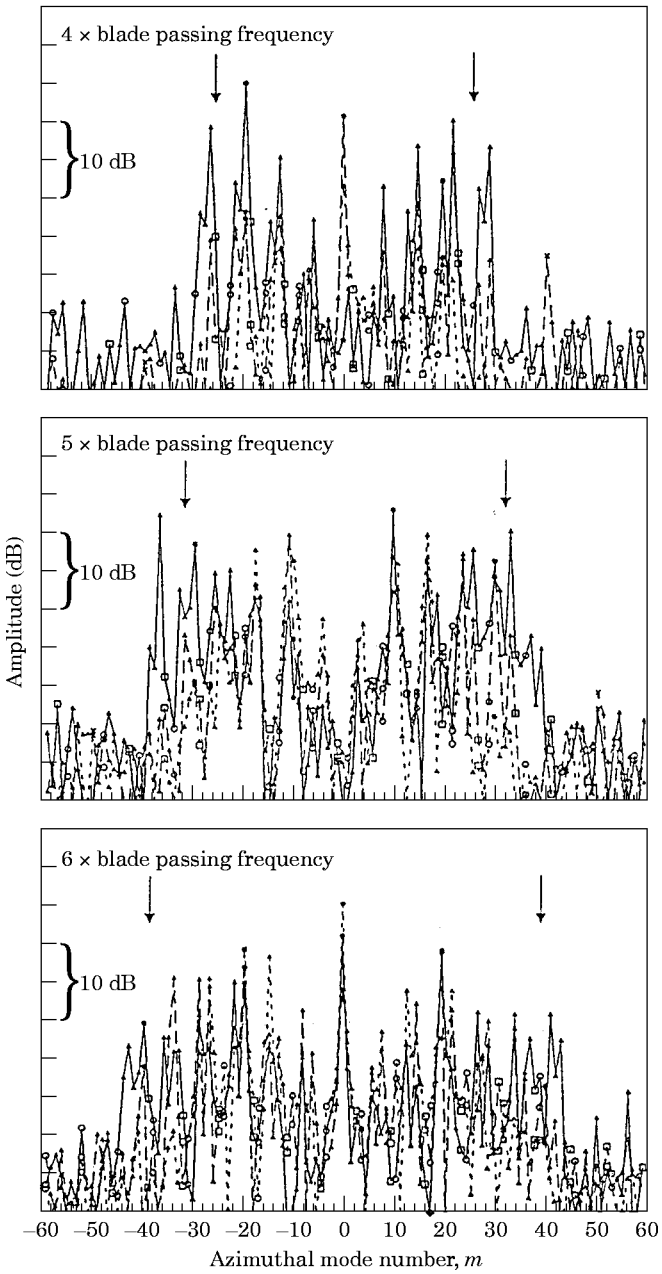

Figure 8. The azimuthal mode distribution for three radial positions for the blade tone harmonics (a) 1–3 and (b) 4–6. Equal blade numbers $B = B_1 = B_2 = 10$; blade tone = $B\Omega = 1762$ Hz ($kR = 6{\cdot}5$), $*$, Rotor 1/rotor 2; ○, rotor 2/struts; □, rotor 1/struts; × rotor 1/rotor 2 and rotor 1/struts or rotor 2/struts; △, other modes. ——, $r = 192$ mm; – – –, $r = 157$ mm; ---, $r = 122$ mm. $\beta = -6^\circ/-6^\circ$; $\pi_{rel} = 1{\cdot}0$; $M = 0{\cdot}22$; $\alpha = 0$.

and one has to assume that both of the possible interaction mechanisms contribute. However, as was shown before for the case of equal blade numbers, knowledge of which of the two possible source mechanisms is more important is not required, insofar as finding ways of noise reduction is concerned, because when the distance between the rotors and

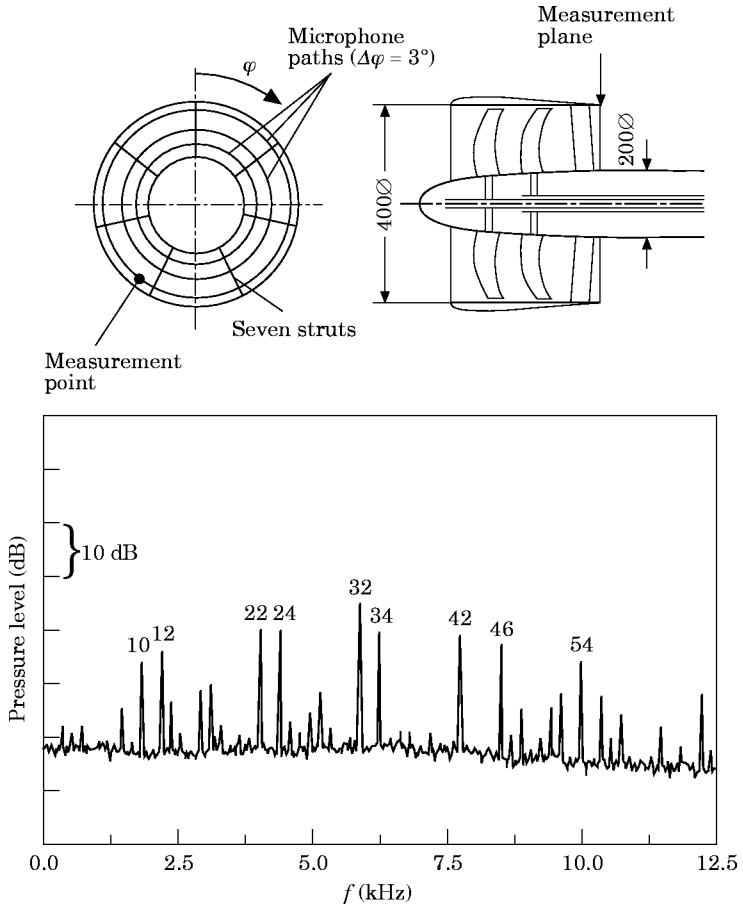

Figure 9. The sound pressure spectrum in the outlet plane for the case of unequal blade numbers; $B_1/B_2 = 10/12$.

the struts is enlarged, the rotor 2/struts interaction mechanism is weakened on the one hand, and on the other hand the non-propagational modes due to the rotor 1/rotor 2 interaction suffer a stronger decay. Both effects lead to a reduced emission of these tone components.

Because of the importance of the blade tones for the overall noise, and to assess the effect of increasing the axial distance between the rotors, the average sound pressure spectrum in the outlet plane was determined from the 360 individual spectra measured at 120 circumferential positions ($\Delta\varphi = 3°$) at $r/R = 0{\cdot}96$, $0{\cdot}785$ and $0{\cdot}61$ radial distances from the rotor axis. In Figures 11(a) and 11(b) are plotted the averaged spectra for the rotor distances $RD = 97{\cdot}3$ mm and $RD = 177{\cdot}3$ mm. The level difference of the two spectra is shown in Figure 11(c). The different shading indicates which interaction mechanism is mainly responsible for the various tone components.

The amplitudes of the shaft harmonic orders $H = 22, 32, 34, 42, 44, \ldots$, which are generated by the two counter-rotating rotrs, are diminished substantially as the distance between the rotors is enlarged. Hardly any change in level is observed for the harmonics $H = 10, 20, \ldots$ and $H = 12, 24, \ldots$, which are due to the rotor 1/struts and rotor 2/struts interactions, respectively. The reason is, of course, that (i) the distance between the second

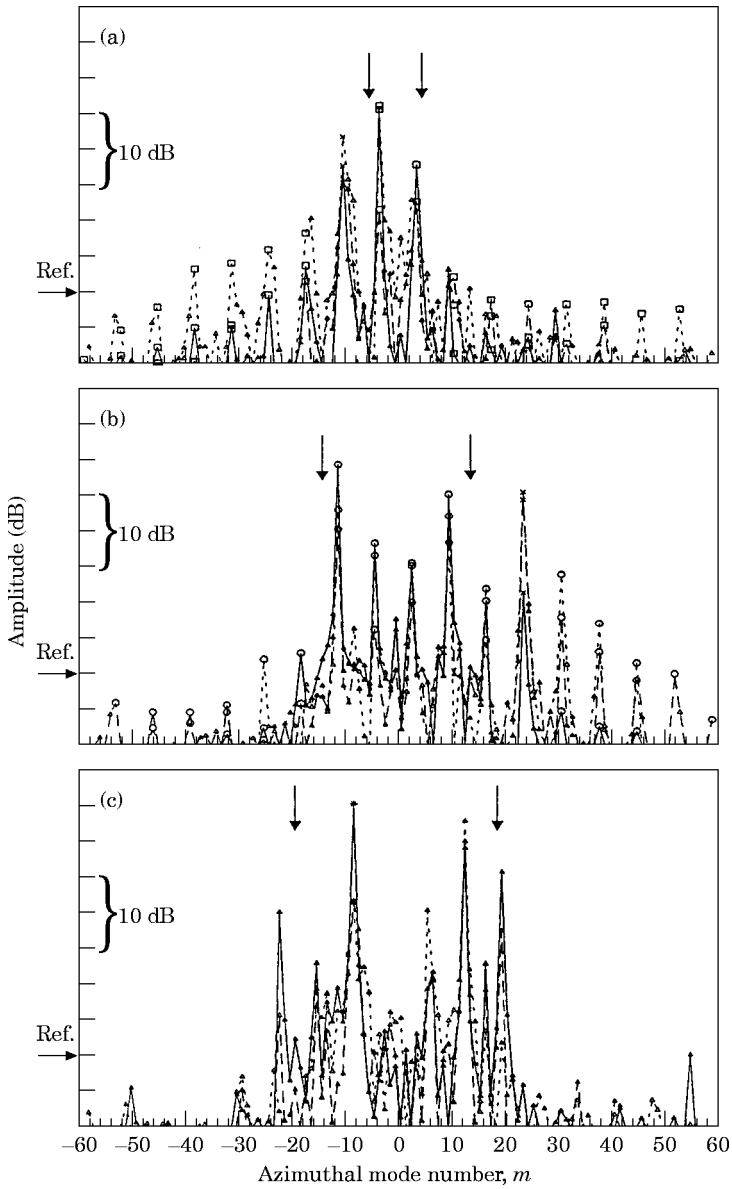

Figure 10. The azimuthal mode distributions of three blade tone components (shaft harmonic orders) for three radial positions; unequal blade number $B_1/B_2 = 10/12$, rotor distance $RD = 97{\cdot}3$ mm; shaft rotational frequency = 186·1 Hz ($kR = 0{\cdot}67$). (a) 10 × rotor shaft frequency; (b) 24 × rotor shaft frequency; (c) 32 × rotor shaft frequency. ∗, Rotor 1/rotor 2; ○, rotor 2/struts; □, rotor 1/struts; ×, rotor 1/rotor 2 and rotor 1/struts or rotor 2/struts; △, other modes. $RD = 97{\cdot}3$ mm; $\beta = -8^\circ/-8^\circ$; $\pi_{rel} = 0{\cdot}8$; $M = 0{\cdot}22$; $\alpha = 0$. ——, $r/R = 0{\cdot}96$; – – –, $r/R = 0{\cdot}785$; ---, $r/R = 0{\cdot}61$.

rotor and the struts was the same in both configurations tested, and hence the interference of the wake flow from the second rotor with the struts remains is nearly unaltered, and (ii) that the distance between the first rotor and the struts was relatively large to start with, so that a further increase has almost no influence on the wake flow in the region of the struts.

4.4. OVERALL HARMONIC PRESSURE LEVEL

To compare the overall tone noise levels of different configurations of the CRISP propfan model at different operating conditions, the levels of all blade tone harmonics, averaged over the cross-section of the exit plane as shown in Figure 11, were summed energetically and are plotted in Figure 12. The black columns denote the levels obtained with the blade numbers $B_1/B_2 = 10/12$ and the enlarged rotor distance $RD = 177{\cdot}3$ mm, the columns shaded horizontally are for the same blade numbers but with the small rotor distance $RD = 97{\cdot}3$ mm, and the pointed shade represents the case of equal blade numbers $B_1 = B_2 = 10$ in combination with the small rotor distance. For the first two cases, the sum was taken over all even harmonics in the range from the second to the 78th. The propfan with ten blades on each rotor generates tone components at every tenth harmonic of the shaft frequency only, and consequently the sum over these was taken in the range $H = 10$–80.

Changing the blade numbers from $B_1/B_2 = 10/10$ to $B_1/B_2 = 10/12$ results in a reduced tone noise level at the relative pressure ratio $\pi_{rel} = 0{\cdot}8$ and a small increase at the pressure ratio $\pi_{rel} = 0{\cdot}4$. Increasing the axial distance between the rotors with $B_1/B_2 = 10/12$ blades reduces the overall tone level by about 8 dB and, thus, proves to be the far more effective

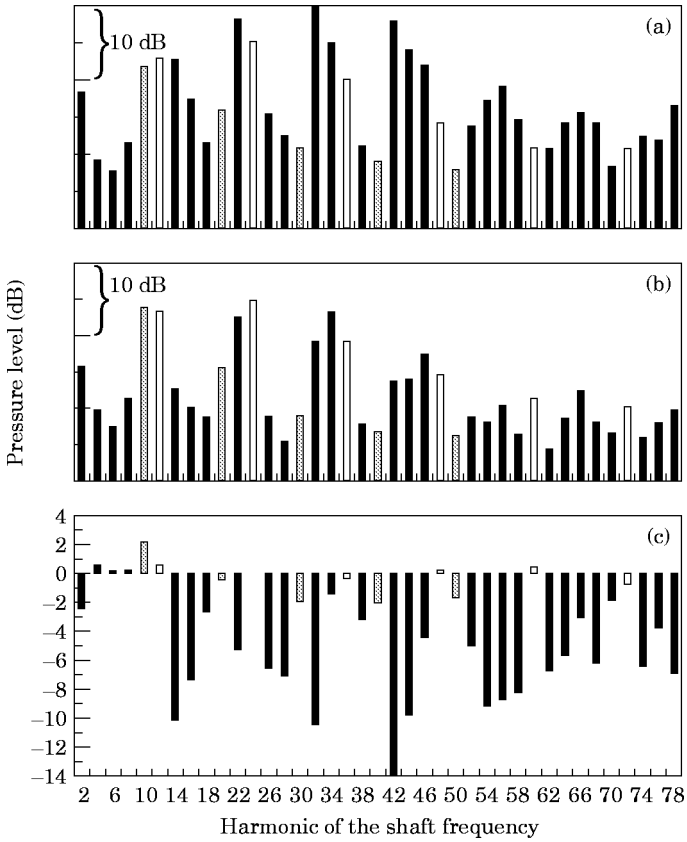

Figure 11. The influence of the axial rotor distance RD on the pressure spectra in the exit plane of the CRISP 0·4 m model (average over 360 measurement points); shaft frequency $\Omega = 186{\cdot}1$ Hz ($kR = 0{\cdot}67$), blade stagger angle $\beta = -8^\circ/-8^\circ$, relative pressure ratio $\pi_{rel} = 0{\cdot}8$, wind tunnel flow $M = 0{\cdot}22$, angle of incidence $\alpha = 0$. (a) $RD = 97{\cdot}3$ mm; (b) $RD = 177{\cdot}3$ mm; (c) difference, $RD = 177{\cdot}3$ mm to $RD = 97{\cdot}3$ mm. ■, Rotor 1/rotor 2; □, rotor 2/struts; ⊡, rotor 1/struts.

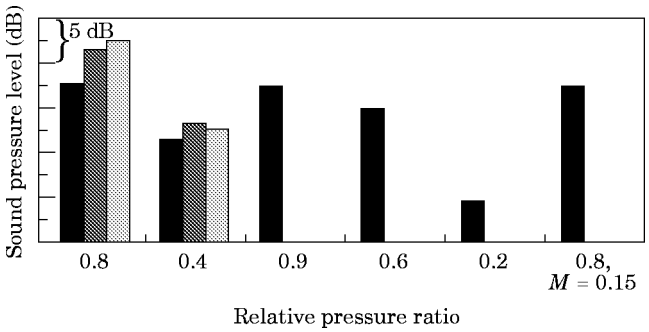

Figure 12. The overall harmonic noise level for different operational conditions of the propfan: rotor distances $RD = 97{\cdot}3$ and $177{\cdot}3$ mm; $B_1/B_2 = 10/12$ and $10/10$; blade stagger angle $\beta = -8^\circ/-8^\circ$; relative pressure ratio $\pi_{rel} = 0{\cdot}9$–$0{\cdot}2$; wind tunnel flow $M = 0{\cdot}22$ and $M = 0{\cdot}15$. ■, 10/12, $RD = 177{\cdot}3$; ▩, 10/12, $RD = 97{\cdot}3$; ▤, 10/10, $RD = 97{\cdot}3$.

noise reduction method. As is to be expected, the tone noise level grows with the relative pressure ratio of the propfan.

4.5. RADIAL MODE DISTRIBUTION

As described in section 2.1, the radial mode amplitudes A_{mn} are calculated from the azimuthal mode distributions obtained at different radial positions. The maximum number of radial modes, which can be determined from the experimental data, is equal to the number of circumferential measurement paths spaced over the duct radius. In this study, measurements were performed on three different radial positions and therefore only the radial modes $n = 0$, 1 and 2 could be determined for each azimuthal mode order m. As an example, in Figure 13 are shown radial mode distributions calculated from the azimuthal mode distribution depicted in Figure 8; i.e., for the case of equal blade numbers $B_1 = B_2 = 10$ and maximum thrust ($\pi_{rel} = 1$). The vertical lines represent the amplitudes of the modes and the different line types indicate the radial mode order n for each value of m. Calculations were carried out only for azimuthal modes m with high amplitudes in the corresponding azimuthal mode distributions.

For most of the azimuthal modes m, not only the radial mode $n = 0$ is found but also the modes $n = 1$, 2, and at some azimuthal mode orders m the amplitudes of the higher order radial modes are larger than those of the modes $n = 0$. It is quite possible that modes with even higher radial mode order exist in the exit plane and, unfortunately, the radial modes with orders $n > 2$ would influence the analyzed radial mode distributions in the range $n \leqslant 2$ due to aliasing. Additional measurements at the radial positions would be necessary to determine the amplitudes of the modes $n > 2$; this was not possible in the present experiments. However, in a study by Holste [1, 2] the tonal noise radiation from the exit plane of the propfan was calculated based on the experimental mode distributions in the range $n \leqslant 2$ and good agreement was found with the results of the independent free field measurements. This indicates that the radial modes of higher order are not important in this case.

The radial mode distributions determined for various operational conditions have similar characteristics, which can be observed in Figure 13. In the case of the second blade tone harmonic, the plane wave mode ($m, n = 0, 0$) is among the dominant modes. Since the plane wave mode is propagational at all frequencies and since the acoustic radiation efficiency of propagational modes is high, one concludes that this mode is mainly responsible for the noise radiation of this tone component. In the acoustic mode distribution of the third blade tone harmonic, the radial modes with the azimuthal order

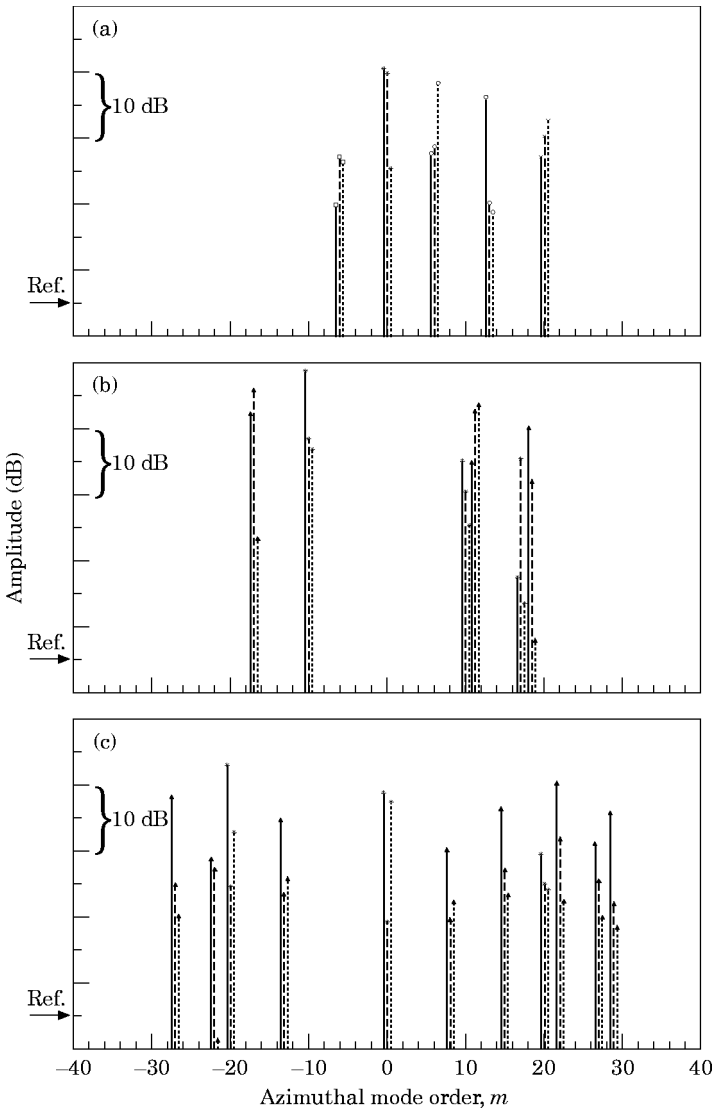

Figure 13. The radial mode distribution of the 2nd to 4th harmonics at maximum thrust; equal blade numbers $B_1 = B_2 = 10$, rotor distance $RD = 97{\cdot}3$ mm; blade passing frequency = 1930 Hz ($kR = 7{\cdot}1$). (a) 2 × blade passing frequency; (b) 3 × blade passing frequency; (c) 4 × blade passing frequency. ∗, Rotor 1/rotor 2; ○, rotor 2/struts; □, rotor 1/struts; ×, rotor 1/rotor 2 and rotor 1/struts or rotor 2/struts; ▲, other modes. ——, $n=0$; ——, $n = 1$; ---, $n = 2$. $\beta = -6^\circ/-6^\circ$; $\pi_{rel} = 1{\cdot}0$; $M = 0{\cdot}22$; $\alpha = 0$.

$m = -10$ are the dominant ones, and together the radial modes with $m = 10$, which rotate in the opposite direction, they form an azimuthal standing wave pattern in the exit plane of the propfan. Such a circumferential pressure distribution was also found in the radiated sound field, as was reported by Dobrzynski *et al*. [7]. The mode distribution of the fourth blade tone harmonic is dominated by the radial mode $n = 0$; this is true for all azimuthal mode numbers: i.e., for the modes generated directly by rotor/rotor interaction as well as for the modes produced indirectly by mode transformation at the struts. Except for the azimuthal mode $m = 0$, the amplitudes of the radial modes $n = 1$ and 2 are very small,

so that one can assume (but not be certain) that the higher radial modes $n > 2$ are also weak.

In summary, it is obvious from the experimental results discussed above that radial modes of high order exist in the exit plane of the propfan and contribute to the noise radiation depending on their acoustic radiation efficiency. These radial modes are generated by the radial variation of the blade profiles, blade loading, mean flow velocity and wakes. As a result, the aerodynamic interaction processes responsible for the tonal the noise components are functions of the radial co-ordinate as well. At the low thrust operating condition, $\pi_{rel} = 0{\cdot}4$, it was found that the radial mode $n = 0$ is dominant for all azimuthal mode orders m. The likely reason for this result is that the rotor speed is low, and with it the frequencies of all tone components, so that most of the radial modes with $n > 0$ are not propagational and occur only with low amplitudes in the exit plane.

5. CONCLUSIONS

Unsteady pressure measurements were performed in the exit plane of the CRISP 0·4 m model to explore the dominant sound generation mechanisms and source regions of the tonal noise components. The propfan model comprises two counter-rotating rotors of 400 mm diameter and a shroud, which is retained by seven struts located downstream of the rotors. The investigations were carried out in co-operation with MTU, who developed the CRISP concept. During the first set of experiments, rotors with ten blades each were used. To reduce the noise, a second measurement series was performed with an unequal number of blades on the rotors ($B_1/B_2 = 10/12$) and with two axial distances between them.

The pressure fluctuations measured in the exit plane were resolved numerically into a distribution of azimuthal modes m, and the azimuthal mode distribution determined for different radial distances from the axis were used to calculate the radial modes A_{mn}, separately for each azimuthal mode order m.

A theoretical analysis is presented which allows one to predict the various tone components and the azimuthal mode orders m generated by the interaction of two rotors with arbitrary blade numbers, speed and direction of rotation. This model can be used to find suitable blade number combinations and rotor speed combinations which generate mainly non-propagational modes, so that the overall noise emission is diminished.

At all operating conditions tested, only those modes were found to exist in the exit plane and to contribute to the radiated noise field, which are propagational in the annular cross-section of the exit.

For the case of equal blade numbers $B_1 = B_2 = 10$, the blade passing frequency component ($H = 10$) is mainly generated by the interaction of the second rotor with the struts and by a transformation of modes while passing through the struts; the interaction between the rotors generates only non-propagational modes at the blade passing frequency. However, at all higher blade tone harmonics ($H = 20, 30, 40, \ldots$) the dominant modes, which are mainly responsible for the noise radiation into the far field, are generated by the rotor 1/rotor 2 interaction. The higher blade tone harmonics were found to have the highest amplitudes in the exit plane as well as in the radiated sound field, and therefore the rotor/rotor interaction is mainly responsible for the overall tone noise level of this test configuration.

Applying the above theoretical analysis to the configuration with $B_1 = 10$ and $B_2 = 12$ blades, yields the result that all even harmonics of the rotor shaft frequency, i.e., $H = 2, 4, 6, \ldots$, can be produced. Furthermore, all rotor harmonics below the order $H = 22$ are generated as acoustic duct modes with high azimuthal mode order m which are not propagational in the annular engine duct, and, therefore, can be expected to have small

amplitudes in the exit plane. The theoretical considerations were confirmed by the measurement results.

For the case of unequal blade numbers, measurements were carried out with two different axial distances between the rotors. With the short distance, the harmonics generated by the rotor/rotor interaction dominate the pressure spectrum averaged over the outlet plane. The amplitudes of these tone components decrease by as much as 8 dB when the axial distance between the rotors is increased from 97·3 mm ($RD/R = 0{\cdot}487$) to 177·3 mm ($RD/R = 0{\cdot}887$). Similar reductions can be expected in the acoustic far field. In case of the large axial rotor distance, the shaft order harmonics generated by the interaction between the rotors and the struts exhibit amplitudes similar to those of the harmonics generated by the rotor/rotor interaction. Hence, for further noise reduction, the axial distance between the rotors and the struts has to be enlarged as well.

Changing the blade numbers from $B_1/B_2 = 10/10$ to $B_1/B_2 = 10/12$ results in a reduction of the overall tone noise levels when the propfan is operated in a condition of large thrust. This experiment was made with the small axial distance between the rotors. The reason for this result is that fewer propagational modes with a high radiation efficiency are generated by the rotor/rotor interaction. In particular, the plane wave mode $m = 0$ is not present in the frequency range of interest.

The radial mode distributions have shown that modes with a higher order than $n = 0$ exist in the exit plane and contribute to the sound radiation, depending on their radiation efficiency.

It was shown that the aerodynamic interaction processes responsible for the blade tone noise of the propfan, i.e., intake flow/rotor 1, rotor 1/rotor 2, rotor 1/struts and rotor 2/struts, generate different sets of azimuthal modes for each tone component. Since the actual mode distributions in the exit plane are known from the acoustic near field measurements and subsequent mode analysis, one is able to conclude what the dominant noise generation mechanisms are for each tone component. Furthermore, knowledge of the mode structure of the sound field in the annulus of the propfan is necessary for the optimum design of acoustic liners for the fan shroud and, also, for efficient application of active noise control measures. Moreover, it was shown by Holste [1, 2] that experimental data obtained in the acoustic near field of the propfan can be used to predict the radiated sound in the acoustic far field very accurately. Since the near field measurements do not require an acoustically ideal test environment, these measurements can also be performed in a conventional test-bed installation, and therefore the experimental techniques presented here, together with Holste's prediction method, can be used to assess the tonal noise characteristics of a new aircraft engine at a very early stage of its development. Naturally, the more detailed the experimental near field data are, the more accurate the predicted far field sound levels and distributions will be. The experimental methods presented here and the prediction method described by Holste [1, 2] were developed and tested on a propfan model; however, they are also applicable to other types of aircraft engines and turbomachines.

REFERENCES

1. F. Holste 1995 16*th Aeroacoustic Conference CEAS/AIAA* 95-103, 729–738. An equivalent source method for calculation of the sound radiated from aircraft engines.
2. F. Holste 1995 *Dissertation*, *TU Berlin*, *VDI-Verlag GmbH*, *Düsseldorf* 1995, *Reihe* 7, *No*. 272. Ermittlung der aerodynamischen Lärmquellen und Berechnung des abgestrahlten Schallfeldes mittels der im Nahfeld gemessenen Druckschwankungen am Beispiel eines Triebwerksmodells.
3. F. Holste and W. Neise 1992 14*th Aeroacoustic Conference DGLR/AIAA* 92-02-138, 826–835.

Experimental determination of the main noise sources in a propfan model by analysis of the acoustic spinning modes in the exit plane.
4. A. MICHALKE 1989 *Journal of Sound and Vibration* **134**, 203–234. On the propagation of sound generated in a pipe of circular cross-section with uniform flow.
5. A. MICHALKE 1990 *Journal of Sound and Vibration* **142**, 311–341. On experimental sound power determination in a circular pipe with uniform mean flow.
6. J. M. TYLER and T. G. SOFRIN 1962 *SAE Transactions* **70**, 309–332. Axial flow compressor noise studies.
7. W. DOBRZYNSKI, B. GEHLHAR and J. BÖTTCHER 1992 14*th Aeroacoustic Conference DGLR/AIAA* 92-02-138, 816–826. Aeroacoustic wind tunnel testing of a counter-rotating shrouded propfan-model.
8. T. ZANDBERGEN, J. N. LAAN and H. J. ZEEMANS 1983 *AIAA*-83-0677. In-flight acoustic measurement in the engine intake of a Fokker F28 aircraft.